ACS APPLIED MATERIALS & INTERFACES

Research Article

www.acsami.org

Biocompatible Fe–Si Nanoparticles with Adjustable Self-Regulation of Temperature for Medical Applications

Ying Jing,[†] Jinming Liu,[†] Wei-Hang Ji,[‡] Wei Wang,[†] Shi-Hai He,[†] Xiao-Ze Jiang,[‡] Timothy Wiedmann,[§] Chun Wang,[‡] and Jian-Ping Wang*[,†]

[†]Department of Electrical and Computer Engineering, [‡]Department of Biomedical Engineering, and [§]Department of Pharmaceutics, University of Minnesota, Minneapolis Minnesota 55455, United States

Supporting Information

ABSTRACT: Because of the noninvasive, locally selective potential of thermal energy, considerable effort has been focused on the use of an external, alternating magnetic field for conversion of magnetic work to heat with iron oxide nanoparticles. However, proper regulation of thermal energy remains a challenge because of the lack of feedback from the local temperature change to the external power supply. Here, we show development of smart magnetic nanoparticles composed of Fe and Si with intrinsically tunable heat generation capability. They were engineered to possess an adjustable magnetic transition temperature through tuning the exchange between Fe atoms by incorporation of silicon atoms. They show relatively high magnetic moment. Moreover, their biocompatibility was established in several cell lines. The nanoparticles were also combined with a thermosensitive polymer, which had the capability to release of molecules with a magnetic stimulus, thereby providing a platform for locally controlled, drug release.

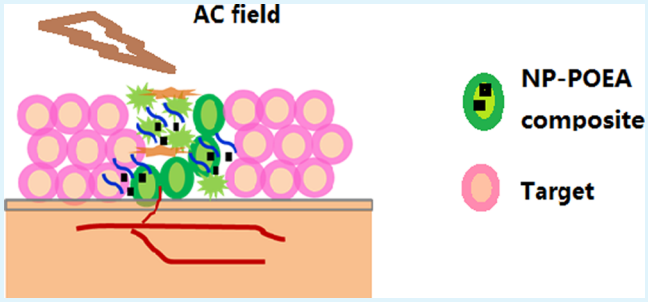

KEYWORDS: *biocompatible magnetic nanoparticles, FeSi nanoparticles, Curie temperature, drug delivery*

INTRODUCTION

Nanotechnology has the potential to revolutionize medical diagnosis and treatment with magnetic nanoparticles (NPs) emerging at the forefront of the field.[1−6] In terms of treatment, NPs enable the localized delivery of thermal energy, which can induce cell death in malignant tumors sensitive to a moderate temperature increase or stimulate the release of drug from temperature-sensitive carriers.[7−11] This approach overcomes the drawbacks of currently available therapies by exposing only the diseased region to activated particles. For such applications, magnetic NPs would ideally work in a designed, narrow temperature range and thereby would have minimal side effects on normal cells.

A major difficulty in achieving the ideal thermal profile in vivo arises from the inability for thermal sensors to map the temperature profile accurately given the small spatial distribution. Nevertheless, it is shown by Huang et al.[12] using fluorophore tags on the surface of magnetite NPs that more than a 15 °C temperature increase can be induced in a very short time at cell surface. While providing quantitative information, this approach does not appear adaptable for manual manipulation of the external electrical power to control the local temperature gradient. Thus, an alternative approach is desired that allows self-regulated heat generation.

One possibility is the use of "smart" NPs that exploit the Curie temperature (T_c) of the magnetic material.[13] It is well-known that the rate of heating slows as the T_c is approached, and no heating occurs at and above this temperature. This has been demonstrated with a number of ferrite materials, such as $La_{1-x}Sr_xMnO_3$,[14] and Zn ferrite.[15] However, these materials suffer from a low saturation magnetization. Since the heating rate is a function of the magnetic moment per particle, which is a product of its magnetization and volume, these ferrites do not produce sufficient heat for biomedical applications. Although it is possible to increase the magnetic moment by doping with rare earth elements,[16] such additions result in particles with unacceptable toxicity. Ni–Cu,[17] Fe–Ni,[18] FeNiZrB,[19] Fe-CoCr,[20] and Ni–Cr[21] are examples of particles with good magnetization but contain toxic elements. A composite particle with a core–shell structure could be employed to enhance the biocompatibility, but significant concerns remain with respect to ensuring complete coverage of the toxic particles as well as the ultimate removal from the body. Thus, producing "smart" NPs composed of biologically acceptable components remains an unrealized goal.

To produce a functional material with intrinsic temperature regulation, we incorporated Si into Fe to produce the desired particles. It is recognized that the T_c is determined by the strength of quantum mechanical exchange-coupling between Fe atoms. Moreover, investigations into bulk samples of Fe–Si

Received: September 22, 2014
Accepted: May 21, 2015
Published: May 21, 2015

DOI: 10.1021/acsami.5b01680
ACS Appl. Mater. Interfaces 2015, 7, 12649−12654

alloys have revealed that hybridization between Fe and Si is possible, and this has an influence on the observed magnetic property. As such, the underlying physics justify the use of Si to reduce T_c of Fe by tuning the interaction through a control of the exchange process.[22] Importantly, Fe[23] and Si[24] are relatively nontoxic and therefore can be expected to be processed to produce a biocompatible material.

For the tuning of Fe−Si composites, it is critical that the mechanism of heat generation be understood as well as the influence of the magnetic properties of NPs. The vanishing magnetic moment of low T_c materials has been addressed, but another important aspect is related to the magnetic anisotropy of NPs. This often overlooked property can be even more sensitive to temperature than that of magnetization.[25] Specifically, when the magnetic anisotropy is outside the optimal heating performance range of the alternating magnetic field, negligible heat is generated.[26] Therefore, in designing Fe−Si NPs, it is critical that both T_c and the temperature-dependent anisotropy be carefully evaluated.

With these principles in mind, we synthesized Fe−Si NPs of different compositions in pursuit of nanoparticles with adjustable temperature-sensitive magnetic properties. A gas phase synthetic method was used to fabricate the Fe−Si NPs, which allowed control on nanoscale of thermal environment for crystal growth, diffusion and segregation,[27,28] and thereby facilitated fabrication of a wide range of NPs. Our synthetic method provides an inherently easy adjustment of composition and exquisite control of the resulting crystalline phase compared to traditional wet-chemical methods.[29]

RESULTS AND DISCUSSION

Figure 1 displays transmission electron microscope (TEM) bright field images of Fe−Si NPs that were prepared with

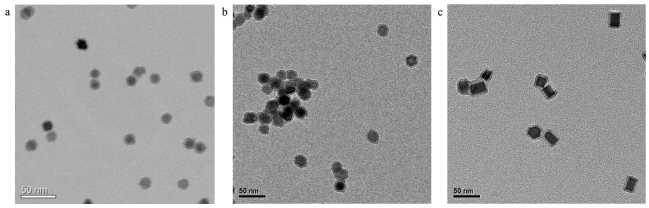

Figure 1. TEM images of Fe−Si NPs with different composition. Bright field TEM images of Fe−Si NPs with (a) 17 atom % Si, (b) 25 atom % Si, and (c) 42 atom % Si.

different ratios of Fe to Si. The particles were mostly multifaceted shaped, with good crystallinity and relatively high uniformity. There is an oxidation shell formed on the surface of nanoparticles. The shell helps passivate the surface so further oxidation can be slowed or prevented. The temperature dependence of saturation magnetization and associated T_c were measured by a vibrating sample magnetometer (VSM). A constant magnetic field of 1 T was applied during measurement. T_c was determined from the tangential slope of the curve at the point of the ferromagnetic transition. It can be seen that T_c decreases as the atomic percentage of Si increased (Figure 2a). A T_c in the range of 373−393 K was found for a Fe−Si NPs composed of 38−42 at% Si. The results demonstrate an effective reduction in T_c and support the premise that T_c can be tuned by incorporating Si into Fe.

To investigate how Si modulates the T_c, the spin-wave stiffness coefficient was assessed from measurements of the

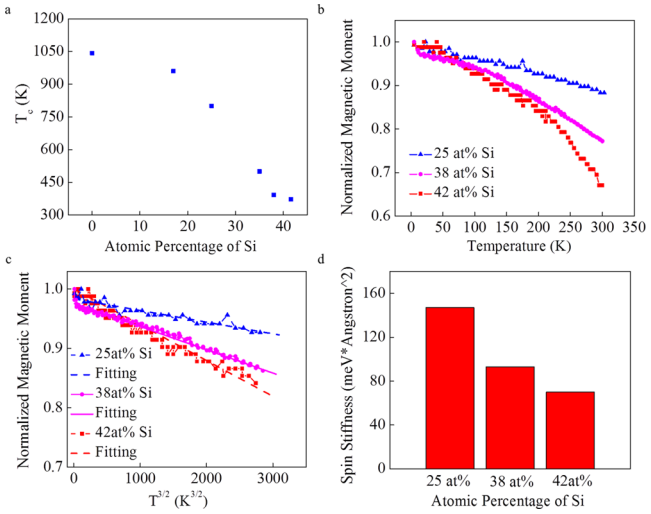

Figure 2. Adjustable T_c of Fe−Si NPs. (a) T_c of Fe−Si nanoparticles as a function of atomic percentage of Si (T_c of Fe was taken from ref 25). (b) Temperature dependence of magnetization from 5 to 300 K. (c) Fitting of curves in panel b based on Bloch's law. (d) Spin stiffness extrapolated from experimental fitting for Fe−Si particles of different composition.

magnetization as a function of temperature for different Si concentrations in the range of 5 to 300 K. The magnetization was evaluated with the spin-wave theory in the frame of Heisenberg's model by fitting the curves to $T^{3/2}$ law in the range of 5−150 K. The results are shown in Figure 2c where the intercept was close to unity (0.97−0.99), and the coefficient of determination was above 90%. Spin-wave stiffness, D, was determined from the spin-wave dispersion relationship $\hbar\omega = Dq^2$ and was calculated from the slope, A,

$$A = 2.612(V/S)(k/4\pi D)^{3/2}$$

where V is the atomic volume of a magnetic atom and S is the spin.[30] The calculated D is given in Figure 2d. A general trend of declining D with increasing atomic percentage of Si is evident. This indicates that the weakening of exchange interactions among Fe atoms is realized by incorporation of Si, and thus T_c is correspondingly tuned. We can conclude that Fe−Si NPs may be engineered for temperature regulation. The T_c of pure iron nanoparticles were not investigated here due to the lack of ultrahigh temperature instrument capability. The T_c of iron nanoparticles should be higher than that of FeSi because of the stronger exchange interactions among the iron atoms.

With the established capability of tuning T_c through a modulation of exchange interactions in Fe−Si, we then focused on NPs of low T_c, which are amenable for self-regulated heat production with potential application in cancer hyperthermia or thermal stimulated drug release. Figure 3a is a TEM bright field image of the cuboidal-shaped NPs with around 38 at% Si. A high magnification image of a single particle is displayed in the inset, and Figure 3b shows the respective selected area diffraction (SAD) pattern. The Fe−Si NPs are highly crystalline as evident from the discrete spots arising from the diffraction of the electron beam by the crystal planes. The SAD pattern also reveals that the NPs are composed of Fe_5Si_3 with a hexagonal structure, consistent with the strong diffraction arising from (002) and (210) crystal planes. High resolution transmission electron microscopy (HRTEM) images of the NPs were used to further characterize the structure, phase information etc. (see

DOI: 10.1021/acsami.5b01680
ACS Appl. Mater. Interfaces 2015, 7, 12649−12654

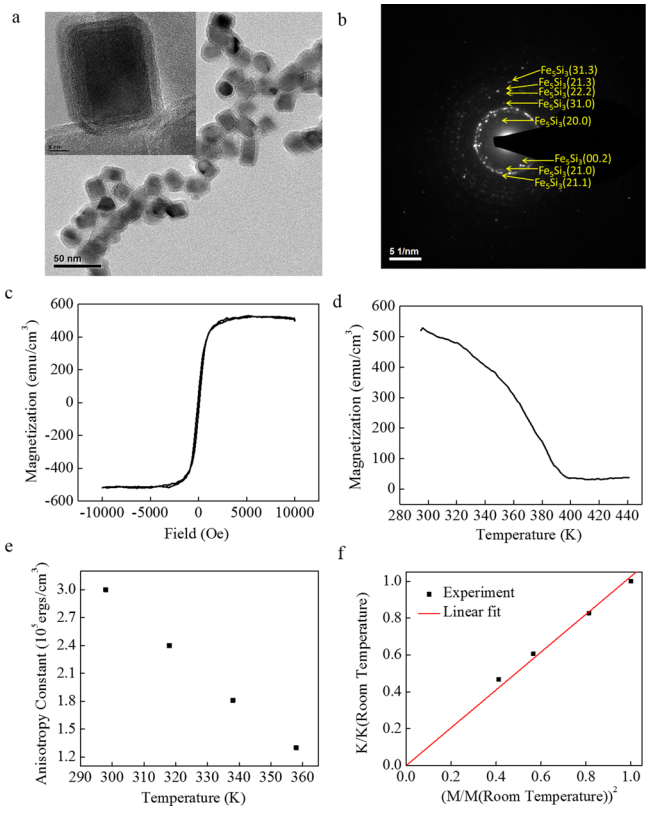

Figure 3. Characterization of Fe−Si NPs. (a) Bright field TEM image of Fe−Si NPs. (b) SAD of Fe−Si NPs. (c) Hysteresis loop of Fe−Si NPs. (d) Temperature dependence of magnetization. (e) Temperature dependence of anisotropy constant. (f) Relationship between temperature dependence of magnetization and anisotropy constant.

Figure S4 in supporting material). The hysteresis loop of an ensemble of NPs was measured by VSM at room temperature (Figure 3c). The saturation magnetization value was calculated based on the magnetic moment and the mass of particles. A value of 80 emu/g was determined which is equivalent to 536 emu/cm^3 using a density of 6.7 g/cm^3. This value is higher than the initially mentioned ferrite materials with low T_c and is comparable to the metallic alloy materials. The remnant magnetic moment of the NPs at zero magnetic field was near 8.5% of saturation magnetic moment, while the coercivity was 70 Oe. It is possible that the remnance and coercivity were a consequence of the interparticle interaction among NPs when packed together onto the substrate. In addition, some large particles in the sample may also contribute to the observed hysteresis. The temperature dependence of magnetization is depicted in Figure 3d. A drop of magnetization takes place as the temperature increases, and a transition at about 393 K is seen. To our knowledge, this is the first demonstration of a low T_c coupled with a relatively high saturation magnetization in a magnetic nanoparticle material that does not contain toxic, heavy metals. The decrease in magnetization will reduce the heating rate, thereby corroborating the claim of self-regulation.

The temperature dependence of the anisotropy constant was also investigated by measurement of the magnetization curves at different temperatures. The anisotropy constant was obtained by extrapolating the magnetization curves based on the law of approach to saturation magnetization for magnetic materials with uniaxial anisotropy.[31] A decrease in the anisotropy constant was found as the temperature increased (Figure 3e), and at room temperature, the effective anisotropy constant was 3×10^5 erg/cm^3. A square power law relationship was deduced by comparing the temperature dependence of anisotropy and magnetization. Figure 3f shows the good fit of the experimental data to the square power law. A similar relationship between magnetization and anisotropy has been observed in other uniaxial materials.[32,33]

Following the characterization of the magnetic properties of the NPs, the cytotoxicity and the rate of magnetic field heating was evaluated. To examine the biocompatibility of PEG coated Fe−Si NPs, the cytotoxicity was tested in cultured mouse embryonic fibroblasts (NIH 3T3) and human umbilical vein endothelial cells (HUVECs) using the standard MTT (3-(4,5-dimethylthiazol-2-yl)-2,5-diphenyltetrazolium bromide) assay. Figure 4a shows that a high percentage of NIH 3T3 cells

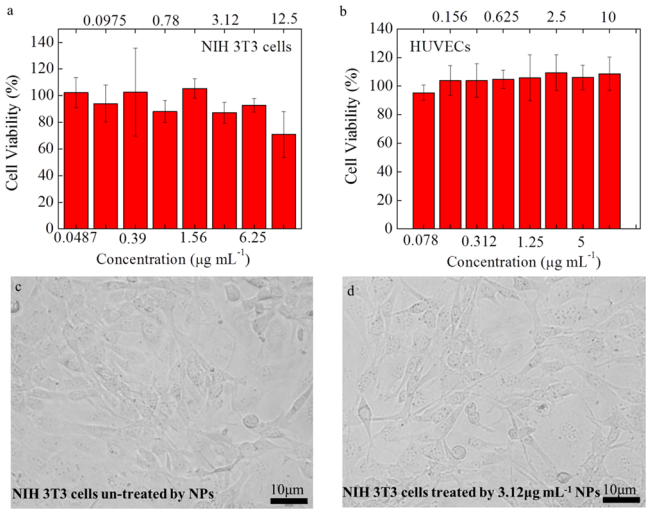

Figure 4. Cytotoxicity of Fe−Si NPs. (a) Viability of mouse embryonic fibroblasts (NIH 3T3) after treatment with Fe−Si NPs at different concentrations. (b) Cytotoxicity result of Fe−Si NPs on HUVECs. (c) Optical image of control cells without loading of Fe−Si NPs. (d) Optical image of cells treated with 3.12 μg mL^{-1} of NPs.

remained viable in concentrations of NP at 6.25 μg/mL. When the concentration of Fe−Si NPs was increased to12.5 μg/mL, the viability dropped to below 80%. Compared to other metallic NPs,[34,35] Fe−Si NPs exhibited lower toxicity. Optical images were also taken of cells without and with the treatment of NPs. By comparing Figure 4c and 4d, the morphology of NIH 3T3 cells remained unchanged within the safe concentration range of NPs. Similar results were observed for HUVECs (Supporting Information Figure S1). A hemolysis test was also carried out with different concentrations of Fe−Si NPs. The results show that particles failed to cause any damage to red blood cells as would be evident by leakage of hemoglobin (Supporting Information Figure S2). Aggregation of blood cells was not observed under the testing conditions. These results indicate that Fe−Si NPs lack overt signs of toxicity, which is a promising indication for their use in medical applications.

Heat generation of Fe−Si NPs under an alternating magnetic field was assessed using a heat sink of 37 °C. The specific loss power (SLP) was calculated from the initial temperature rise as a function of time.[36] For the Fe−Si NPs suspended in phosphate buffered saline (PBS) pH = 7.4, a SLP of about 209 W/g was obtained under an alternating magnetic field of 380 kHz and 40 Oe (Supporting Information Figure S3). To test

DOI: 10.1021/acsami.5b01680
ACS Appl. Mater. Interfaces 2015, 7, 12649−12654

the possibility of using these particles for thermally stimulated drug delivery, a heating experiment was also performed in which the NPs were incorporated into a thermosensitive copolymer. A poly(ortho ester amides) (POEA) copolymer was synthesized according to a published method.[37] The synthesis process of the POEA copolymer and its property control could be found in the ref 37. A gel−sol transition temperature at about 45 °C was obtained for the application purpose in this paper. A composite sample was prepared by incorporating Fe−Si NPs and a fluorescein Rhodamine B dye into the POEA gel. The oxide shell of the FeSi nanoparticles can form hydrogen bonding between the nanoparticles and POEA copolymer avoiding the loosely wrap between the nanoparticles and the dye. A sample of POEA gel loaded with only dye was also prepared as a control. Figure 5a and 5c show the photographs

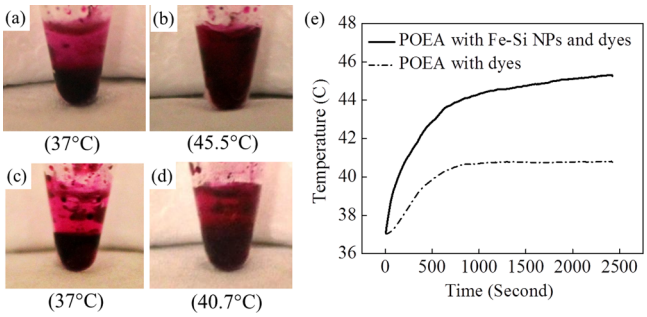

Figure 5. Dye release under magnetic field heating by POEA/Fe−Si NPs composite. Photos of POEA copolymer loaded with Fe−Si NPs and dyes (a) before applying the magnetic field at 37 °C and (b) after applying the magnetic field. Photos of POEA copolymer loaded with dyes (c) before applying the magnetic field at 37 °C and (d) after applying the magnetic field. (e) Temperature rise versus time for POEA copolymer loaded with Fe−Si NPs and dyes and POEA copolymer loaded with dyes only.

of the sample with NPs and without NPs respectively before the magnetic field was turned on. Figure 5b and 5d show the ending status of the sample with NPs and without NPs respectively after the magnetic field was applied. In Figure 5a, a clear difference of color can be seen between PBS buffer and the composite gel, which suggests that the dye is mostly entrapped within the gel. The temperature change of the composite during magnetic field heating was recorded and is displayed in Figure 5e. The FeSi nanoparticles can generate heat to help increase the temperature when the AC magnetic field applied and then the composite gradually heats to the transition temperature of the copolymer. Upon reaching the transition temperature, the gel dissolves into the PBS buffer and the dye was completely released into the solution. During this process, the gel undergoes sol−gel transition as the temperature increases to its phase transition temperature. The sol is dispersed into PBS solvent. The final solution has a uniformly dark red color from the released dye as shown in Figure 5b. In comparison, the control sample without NPs had an increase of temperature of about 3 °C (Figure 5e). Before and after magnetic field heating, a clear difference in color exists between the PBS buffer and the composite (Figure 5c and 5d), which indicates that the gel did not dissolve in the absence of NPs. The slight change in color of the PBS buffer before and after heating was likely due to passive diffusion of dye molecules from the surface of the composite. Overall, this experiment provides proof of concept of the potential of Fe−Si NPs for thermally stimulated drug delivery.

CONCLUSION

In summary, an innovative approach was used to prepare biocompatible "smart" magnetic NPs for self-regulated therapeutic applications. Fe−Si NP system was used to demonstrate that a lower T_c can be achieved through tuning of exchange interaction. The lower T_c correlates with the weakening of exchange interaction as a consequence of the higher content of Si. Particles with composed of Fe_5Si_3 in a crystalline phase had a low T_c but retained a high magnetic moment. Thus, these NPs represent a good candidate for self-regulated thermal therapy. The NPs had relative low toxicity in cell cultures and demonstrated excellent heat generation that induced a phase transition in thermal sensitive copolymers resulting in enhanced drug release. This work provides insights on a new type of biocompatible magnetic NPs with self-regulation of temperature.

METHODS

Synthesis of NPs. Fe−Si magnetic NPs were synthesized by a magnetron sputtering based nanocluster deposition system.[27,28] Vapor of atoms was generated from the composite Fe−Si target by the sputtering gun. During the synthesis, sputtering current was in the range of 0.4−0.6 A. The pressure in the nanocluster source was varied between 40 and 70 Pa by Ar gas feeding. The pressure in the deposition chamber was below 0.1 Pa. NPs were collected onto Si substrates, amorphous carbon-coated Cu grids and PEG-coated glass substrates for further experimental investigation. Quite a few types of nanoparticles prepared by our group have been using PEG coating method.[38,39] This method can provide reasonable dispersion and have be applied on different kinds of nanoparticles.

Sample Characterization. The morphology and structure of the NPs were examined by TEM (FEI T12) and HRTEM (FEI G2 30). A VSM (Princeton measurements) equipped with a flowing helium gas furnace was used to probe magnetic properties at 300−800 K. A magnetic property measurement system (Quantum Design, MPMS XL) was used to carry out the magnetic measurements at 5−300 K. The concentration of NP solution was determined by inductively coupled plasma spectrometry (ICP).

Alternating Magnetic Field Heating. The alternating magnetic field was generated by an induction coil system (Hyperthermia Inc.). The experimental samples were placed in the center of the coil with insulation wraps. The temperature change was monitored by a fluoroptic thermometry system (Luxtron 3100, Lumasense Technologies) and recorded by a computer.

Preparation of Thermal Sensitive Gel with NP Loading. A sample containing 0.015 g of POEA copolymer was heated above the transition temperature to form the sol. Concentrated Fe−Si NPs and 0.001 g of Rhodamine B dyes in PBS were mixed with the sol. A control sample was made with only POEA and dyes in a similar manner. The sample was cooled down under shaking to form a gel. The concentration of NP was 0.5 wt % measured by ICP.

ASSOCIATED CONTENT

Supporting Information

Cytoxicity, hemolysis results, magnetics field heating, high resolution TEM images, EDX data, and size distribution. The Supporting Information is available free of charge on the ACS Publications website at DOI: 10.1021/acsami.5b01680.

DOI: 10.1021/acsami.5b01680
ACS Appl. Mater. Interfaces 2015, 7, 12649−12654

AUTHOR INFORMATION

Corresponding Author

*Address: Department of Electrical and Computer Engineering, University of Minnesota, 200 Union Street SE, Minneapolis, MN 55455. E-mail: jpwang@umn.edu.

Author Contributions

Y.J. and J.-P.W. synthesized and characterized nanoparticles, carried out magnetic field heating experiments, dye release experiment, and wrote the paper. J.L. contributed to the nanoparticle fabrication and manuscript preparation. W.J. and C.W. synthesized POEA polymers, performed cytotoxicity experiments, and dye release experiment. T.W. contributed to magnetic field heating experiments and preparation of the manuscript.

Notes

The authors declare no competing financial interest.

ACKNOWLEDGMENTS

Parts of this work were carried out in using the Characterization Facility, which receives partial support from NSF through the NSF Minnesota MRSEC program under Award Number DMR-0819885. The authors thank the partial support from the Institute of Engineering in Medicine and the Institute for Rock Magnetism, University of Minnesota, for the use of instruments. The authors thank Dr. Yunhao Xu for enlightening discussions.

REFERENCES

(1) Lee, J.-H.; Jang, J.-T.; Choi, J.-S.; Moon, S. H.; Noh, S.-H.; Kim, J.-W.; Kim, J.-G.; Kim, I.-S.; Park, K. I.; Cheon, J. Exchange-Coupled Magnetic Nanoparticles for Efficient Heat Induction. *Nat. Nanotechnol.* **2011**, *6*, 418−422.

(2) Zabow, G.; Dodd, S.; Moreland, J.; Koretsky, A. Micro-Engineered Local Field Control for High-Sensitivity Multispectral MRI. *Nature* **2008**, *453*, 1058−1063.

(3) Kim, D.-H.; Rozhkova, E. a; Ulasov, I. V.; Bader, S. D.; Rajh, T.; Lesniak, M. S.; Novosad, V. Biofunctionalized Magnetic-Vortex Microdiscs for Targeted Cancer-Cell Destruction. *Nat. Mater.* **2010**, *9*, 165−171.

(4) Basly, B.; Felder-Flesch, D.; Perriat, P.; Pourroy, G.; Bégin-Colin, S. Properties and Suspension Stability of Dendronized Iron Oxide Nanoparticles for MRI Applications. *Contrast Media Mol. Imaging* **2011**, *6*, 132−138.

(5) Wang, Y.; Wu, G.; Li, X.; Wang, Y.; Gao, H.; Ma, J. On−Off Switchable Drug Release from Multi-Responsive Degradable Poly-(Ether Urethane) Nanoparticles. *Biomater. Sci.* **2013**, *1*, 614−624.

(6) Wang, H.; Mararenko, A.; Cao, G.; Gai, Z.; Hong, K.; Banerjee, P.; Zhou, S. Multifunctional 1D Magnetic and Fluorescent Nanoparticle Chains for Enhanced MRI, Fluorescent Cell Imaging, and Combined Photothermal/chemotherapy. *ACS Appl. Mater. Interface* **2014**, *6*, 15309−15317.

(7) Guardia, P.; Di Corato, R.; Lartigue, L.; Wilhelm, C.; Espinosa, A.; Garcia-Hernandez, M.; Gazeau, F.; Manna, L.; Pellegrino, T. Water-Soluble Iron Oxide Nanocubes with High Values of Specific Absorption Rate for Cancer Cell Hyperthermia Treatment. *ACS Nano* **2012**, *6*, 3080−3091.

(8) Mikhaylov, G.; Mikac, U.; Magaeva, A. a; Itin, V. I.; Naiden, E. P.; Psakhye, I.; Babes, L.; Reinheckel, T.; Peters, C.; Zeiser, R.; Bogyo, M.; Turk, V.; Psakhye, S. G.; Turk, B.; Vasiljeva, O. Ferri-Liposomes as an MRI-Visible Drug-Delivery System for Targeting Tumours and Their Microenvironment. *Nat. Nanotechnol.* **2011**, *6*, 594−602.

(9) Martinez-Boubeta, C.; Simeonidis, K.; Serantes, D.; Conde-Leborán, I.; Kazakis, I.; Stefanou, G.; Peña, L.; Galceran, R.; Balcells, L.; Monty, C.; Baldomir, D.; Mitrakas, M.; Angelakeris, M. Adjustable Hyperthermia Response of Self-Assembled Ferromagnetic Fe−MgO Core−Shell Nanoparticles by Tuning Dipole−Dipole Interactions. *Adv. Funct. Mater.* **2012**, *22*, 3737−3744.

(10) Wang, H.; Yi, J.; Mukherjee, S.; Banerjee, P.; Zhou, S. Magnetic/NIR-Thermally Responsive Hybrid Nanogels for Optical Temperature Sensing, Tumor Cell Imaging and Triggered Drug Release. *Nanoscale* **2014**, *6*, 13001−13011.

(11) Chen, L.; Li, L.; Zhang, H.; Liu, W.; Yang, Y.; Liu, X.; Xu, B. Magnetic Thermosensitive Core/shell Microspheres: Synthesis, Characterization and Performance in Hyperthermia and Drug Delivery. *RSC Adv.* **2014**, *4*, 46806−46812.

(12) Huang, H.; Delikanli, S.; Zeng, H.; Ferkey, D. M.; Pralle, A. Remote Control of Ion Channels and Neurons through Magnetic-Field Heating of Nanoparticles. *Nat. Nanotechnol.* **2010**, *5*, 602−606.

(13) Wang, S. X.; Taratorin, A. M.. *Magnetic Information Storage Technology*; Academic Press: San Diego, CA, 1999.

(14) Pollert, E.; Knížek, K.; Maryško, M.; Kašpar, P.; Vasseur, S.; Duguet, E. New Tc-Tuned Magnetic Nanoparticles for Self-Controlled Hyperthermia. *J. Magn. Magn. Mater.* **2007**, *316*, 122−125.

(15) Brusentsova, T. N.; Brusentsov, N. a.; Kuznetsov, V. D.; Nikiforov, V. N. Synthesis and Investigation of Magnetic Properties of Gd-Substituted Mn−Zn Ferrite Nanoparticles as a Potential Low-TC Agent for Magnetic Fluid Hyperthermia. *J. Magn. Magn. Mater.* **2005**, *293*, 298−302.

(16) Brusentsova, T. N.; Kuznetsov, V. D. Synthesis and Investigation of Magnetic Properties of Substituted Ferrite Nanoparticles of Spinel System $Mn_{1-x}Zn_x[Fe_{2-y}L_y]O_4$. *J. Magn. Magn. Mater.* **2007**, *311*, 22−25.

(17) Chatterjee, J.; Bettge, M.; Haik, Y.; Jen Chen, C. Synthesis and Characterization of Polymer Encapsulated Cu−Ni Magnetic Nanoparticles for Hyperthermia Applications. *J. Magn. Magn. Mater.* **2005**, *293*, 303−309.

(18) McNerny, K. L.; Kim, Y.; Laughlin, D. E.; McHenry, M. E. Chemical Synthesis of Monodisperse Γ-Fe−Ni Magnetic Nanoparticles with Tunable Curie Temperatures for Self-Regulated Hyperthermia. *J. Appl. Phys.* **2010**, *107*, 09A312.

(19) Ipus, J. J.; Ucar, H.; McHenry, M. E. Near Room Temperature Magnetocaloric Response of an (FeNi)ZrB Alloy. *IEEE Trans. Magn.* **2011**, *47*, 2494−2497.

(20) Miller, K. J.; Colletti, a.; Papi, P. J.; McHenry, M. E. Fe−Co−Cr Nanocomposites for Application in Self-Regulated Rf Heating. *J. Appl. Phys.* **2010**, *107*, 09A313.

(21) Akin, Y.; Obaidat, I. M.; Issa, B.; Haik, Y. $Ni_{1-x}Cr_x$ Alloy for Self Controlled Magnetic Hyperthermia. *Cryst. Res. Technol.* **2009**, *44*, 386−390.

(22) Seo, W. S.; Lee, J. H.; Sun, X.; Suzuki, Y.; Mann, D.; Liu, Z.; Terashima, M.; Yang, P. C.; McConnell, M. V.; Nishimura, D. G.; Dai, H. FeCo/graphitic-Shell Nanocrystals as Advanced Magnetic-Resonance-Imaging and near-Infrared Agents. *Nat. Mater.* **2006**, *5*, 971−976.

(23) Hadjipanayis, C. G.; Bonder, M. J.; Balakrishnan, S.; Wang, X.; Mao, H.; Hadjipanayis, G. C. Metallic Iron Nanoparticles for MRI Contrast Enhancement and Local Hyperthermia. *Small* **2008**, *4*, 1925−1929.

(24) Erogbogbo, F.; Yong, K.-T.; Hu, R.; Law, W.-C.; Ding, H.; Chang, C.-W.; Prasad, P. N.; Swihart, M. T. Biocompatible Magnetofluorescent Probes: Luminescent Silicon Quantum Dots Coupled with Superparamagnetic Iron(III) Oxide. *ACS Nano* **2010**, *4*, 5131−5138.

(25) O'Handley, R. C. *Modern Magnetic Materials: Pinciples and Applications*; John Wiley and Sons Ltd.: New York, 1999.

(26) Sohn, H.; Victora, R. H. Optimization of Magnetic Anisotropy and Applied Fields for Hyperthermia Applications. *J. Appl. Phys.* **2010**, *107*, 09B312.

(27) Qiu, J.-M.; Wang, J.-P. Tuning the Crystal Structure and Magnetic Properties of FePt Nanomagnets. *Adv. Mater.* **2007**, *19*, 1703−1706.

(28) Xu, Y.-H.; Wang, J.-P. Direct Gas-Phase Synthesis of Heterostructured Nanoparticles through Phase Separation and Surface Segregation. *Adv. Mater.* **2008**, *20*, 994−999.

DOI: 10.1021/acsami.5b01680
ACS Appl. Mater. Interfaces 2015, 7, 12649−12654

(29) Kolel-veetil, M. K.; Qadri, S. B.; Osofsky, M.; Goswami, R.; Keller, T. M. Carbon Nanocapsule-Mediated Formation of Ferromagnetic Fe_5Si_3 Nanoparticles. *J. Phys. Chem. C* **2009**, 14663−14671.
(30) Zhang, M.; Brück, E.; De Boer, F. R.; Li, Z.; Wu, G. The Magnetic and Transport Properties of the Co_2FeGa Heusler Alloy. *J. Phys. D. Appl. Phys.* **2004**, *37*, 2049−2053.
(31) McCallum, R. W. Determination of the Saturation Magnetization, Anisotropy Field, Mean Field Interaction, and Switching Field Distribution for Nanocrystalline Hard Magnets. *J. Magn. Magn. Mater.* **2005**, *292*, 135−142.
(32) Okamoto, S.; Kikuchi, N.; Kitakami, O.; Miyazaki, T.; Shimada, Y.; Fukamichi, K. Chemical-Order-Dependent Magnetic Anisotropy and Exchange Stiffness Constant of FePt (001) Epitaxial Films. *Phys. Rev. B* **2002**, *66*, 24413.
(33) Margeat, O.; Tran, M.; Spasova, M.; Farle, M. Magnetism and Structure of Chemically Disordered $FePt_3$ Nanocubes. *Phys. Rev. B* **2007**, *75*, 134410.
(34) Xu, C.; Yuan, Z.; Kohler, N.; Kim, J.; Chung, M. A. FePt Nanoparticles as an Fe Reservoir for Controlled Fe Release and Tumor Inhibition. *J. Am. Chem. Soc.* **2009**, *131*, 15346−15351.
(35) Hu, M.-J.; Lu, Y.; Zhang, S.; Guo, S.-R.; Lin, B.; Zhang, M.; Yu, S.-H. High Yield Synthesis of Bracelet-like Hydrophilic Ni−Co Magnetic Alloy Flux−Closure Nanorings. *J. Am. Chem. Soc.* **2008**, *130*, 11606−11607.
(36) Rosensweig, R. E. Heating Magnetic Fluid with Alternating Magnetic Field. *J. Magn. Magn. Mater.* **2002**, *252*, 370−374.
(37) Tang, R.; Palumbo, R. N.; Ji, W.; Wang, C. Poly(Ortho Ester Amides): Acid-Labile Temperature-Responsive Copolymers for Potential Biomedical Applications. *Biomacromolecules* **2009**, *10*, 722−727.
(38) Srinivasan, B.; Li, Y.; Jing, Y.; Xu, Y.; Yao, X.; Xing, C.; Wang, J.-P. A Detection System Based on Giant Magnetoresistive Sensors and High-Moment Magnetic Nanoparticles Demonstrates Zeptomole Sensitivity: Potential for Personalized Medicine. *Angew. Chem.* **2009**, *121*, 2802−2805.
(39) Kline, T. L.; Xu, Y.; Jing, Y.; Wang, J. Biocompatible High-Moment FeCo−Au Magnetic Nanoparticles for Magnetic Hyperthermia Treatment Optimization. *J. Magn. Magn. Mater.* **2009**, *321*, 1525−1528.

DOI: 10.1021/acsami.5b01680
ACS Appl. Mater. Interfaces 2015, 7, 12649−12654